Robotics: Science and Systems 2026
Sydney, Australia, July 13–17, 2026

High Precision Hydraulic Excavator Control for Heavy-Duty Grading

Lennart Werner[1], Pol Eyschen[1], Sean Costello[2], Andrei Cramariuc[1] and Marco Hutter[1]
[1]ETH Zürich, Robotic Systems Lab, Zürich, Switzerland
[2]Hexagon AB, Heerbrugg, Switzerland
Email: {lennartwerner, peyschen, crandrei, mahutter}@ethz.ch, sean.costello@hexagon.com

***Abstract*—High-precision heavy-duty grading is a common step in earthworks, traditionally carried out manually by skilled operators. Removing a significant amount of material while achieving a high-precision surface requires substantial machine-specific experience. Different hydraulic architectures react differently to operator inputs and soil interaction forces, which makes generalizable controllers challenging. In this paper, we present an autonomous controller that achieves high-precision grading at expert-operator speed on Load Sensing and Negative Flow Control machines alike. We split our controller into two parts: (1) a hydraulic-aware low-level loop that is hydraulic architecture-specific and (2) a path-tracking layer that coordinates joint motions and responses. Through a calibration process, our technique is applicable to load-sensing and negative-flow-control machinery. To showcase its versatility, we benchmark our approach on two excavators with different hydraulics and compare it against a commercial state-of-the-art solution. Our technique (RMSE 1.8 cm) outperforms the commercial solution (RMSE 4.7 cm) in precision by a factor of 2.6 and improves machine usage by leveraging the maximum function pressure, as opposed to commercial solutions that stall prematurely.**

I. Introduction

Despite significant progress in industrial automation, heavy machinery on construction sites is still largely operated manually. Operators are exposed to hazardous environments and face high physical and cognitive loads. At the same time, the industry struggles to meet demand due to persistent labor shortages. Intelligent assistive systems and automation for heavy equipment can enable safer, more consistent, and more efficient operation, especially for users with limited experience. Yet automating earthmoving tasks such as digging, trenching, and grading is difficult due to the complex coupling between the soil and the machine as well as the high complexity associated with precision hydraulic control. In particular, high-precision tasks such as grading require substantial operator experience and are time-consuming to perform.

In this paper, we address autonomous high-accuracy grading with substantial ground interaction, as shown in Figure 1 and in our supplementary video[1]. We propose a technique that generalizes across excavators and hydraulic architectures such as Load Sensing (LS) and Negative Flow Control (NFC). We define heavy-duty grading as cuts that fill the bucket in less than one stroke. Current commercial systems perform poorly in deep grading, stall before the maximum function pressure is reached, and deviate from the target surface. State-of-the-art Inverse Kinematics (IK)-based methods also lose accuracy across soils, since joint responses are load-dependent and are not fully modeled [32]. Prior work has not shown real in-soil centimeter-level grading that combines soft hydraulic actuation, load-dependent compensation, short calibration, and transfer across hydraulic architectures.

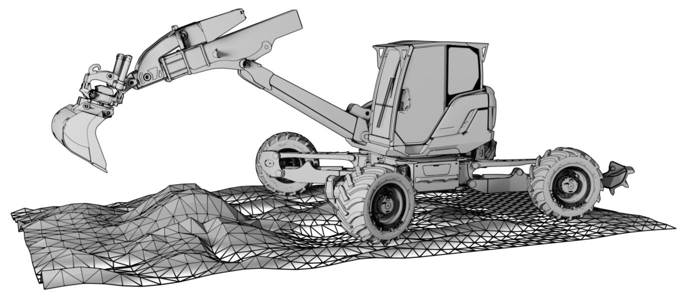

Fig. 1. Heavy-duty grading with the Menzi Muck M445. Grading denotes the removal of uneven ground to form a prescribed planar surface. In the shown setting, this requires substantial soil interaction while maintaining the bucket edge on the target plane. The proposed retrofittable, hydraulics-aware controller automates such in-soil grading passes across excavators and achieves centimeter-level surface accuracy.

We propose a retrofittable[2], machine-agnostic[3] controller for LS and NFC hydraulic excavators. It combines NFC-specific hydraulic compensation for soft, load-dependent actuation, a fast one-time calibration without vendor-specific access, and a Model Predictive Control (MPC) path-tracking layer for precise in-soil grading under varying load. LS hydraulics are modeled with a simple mapping between Directional Control Valve (DCV) displacement and function flow, while NFC machines require a load-dependent function flow model. We introduce a new NFC model that accurately inverts the hydraulically soft behavior and matches the target function flow under load. Velocity transients are modeled as a second-order system with added dead time for the MPC path tracking.

We validate the method on two excavators with different weight classes and hydraulics. Velocity tracking experiments show that the calibrated hydraulic models match target joint rates under varying loads. We compare in-soil deep grading performance to a commercial state-of-the-art system. In a

[1]https://youtu.be/bCOMYbRWv5I

[2]can be calibrated without vendor-specific access

[3]generalizes across machines without changes to the method

test campaign on the NFC excavator, our controller achieves an RMSE height error of 1.8 cm at different cutting depths, compared to 4.7 cm for the commercial system. Experiments on the 11.5 t LS machine confirm a precision of 1.4 cm across various cutting depths. We assess surface quality and precision of the graded areas with a high-precision laser scanner. The proposed system stalls only at the maximum function pressure, unlike commercial controllers, which stall earlier, thereby under-utilizing the machinery. Our framework presents a significant advance in grading quality, enabling direct use of the prepared terrain. In our tested setting, the commercial system required additional passes to reach comparable surface quality.

In sum, the contributions of this paper are:

- A hydraulics-aware control stack for heavy-duty high-precision grading that achieves 2.6 times lower error than the baseline.
- A novel pressure-adaptive NFC model that compensates soft, load-dependent hydraulic actuation.
- A one-time retrofit calibration routine and path-tracking layer that achieve sub-2 cm in-soil grading.

II. Related Work

Automation of earthmoving equipment has been investigated from early assistive systems to fully autonomous platforms. Reviews of earthmoving automation and construction robotics summarize sensing, perception, and control approaches across excavators, wheel loaders, and bulldozers, and highlight the trend toward tighter integration of machine control with digital site models and fleet-level planning [2, 22].

A. Automation of Heavy Machinery

Robotic excavation has progressed from early research prototypes to full-scale autonomous machines. Free-form trenching and foundation work is demonstrated using a walking excavator in [14]. Autonomous short-cycle loading with standard tracked excavators has been shown in a complete system that performs material loading in a quarry, including perception, planning, and robust execution in varied terrain [33]. Recent work on excavation planning extends these results to higher-level task and motion planning for bulk earth removal [25].

Beyond excavators, autonomous and semi-autonomous wheel loaders and haul trucks have been studied for mining and earthworks. Simulation-based optimization and, more recently, learned world models are used to tune loading cycles and bucket trajectories under granular material interaction [1]. These systems focus on productivity and cycle time and typically rely on proprietary machine-control layers tuned to a specific hydraulic architecture and task.

B. Hydraulic Motion Control

Hydraulic excavator motion control research spans physics-based modeling, optimization, and learned abstractions. A complete grading pipeline with perception, stroke planning, and motion control is presented by Jang et al. [12]. On the modeling side, Kim et al. [15] derive a nonlinear DCV model capturing internal switching, joint coupling, and shared pump-flow constraints, and use constrained optimization to scale the desired bucket motion under flow saturation.

Learning-based and reduced-order approaches often trade modeling effort for data or structural assumptions. Lee et al. [18] learn an inverse mapping from desired joint velocities to valve commands with delay compensation, reporting ≈ 2 cm tracking after several hours of machine-specific data collection. Wang et al. [27] propose an observer-based approximate affine nonlinear MPC to improve tracking with reduced computational cost, and Msaad et al. [21] apply data-driven nonlinear MPC via local model networks for grading on a single machine and hydraulic architecture.

Reinforcement-learning methods have been tested on full-scale hydraulic machines, including sim-to-real trajectory control [7], end-to-end bucket filling for soil manipulation [8], offline Reinforcement Learning (RL) for rigid-object excavation [13, 20], and learned rock or bulk manipulation [10]. For grading, Kim and Kim [16] use RL to tune a neural-network inversion layer, while Spinelli et al. [23] and Werner et al. [29] control hydraulic material-handling machines with underactuated tools. In our preliminary light-grading tests, an end-to-end RL policy reached about 6 cm tracking error. It relied on a task-specific simulator and did not handle load-dependent NFC hydraulics or transfer across excavators.

Overall, model-based and data-driven motion controllers can be accurate, but most assume one hydraulic topology, abstract hydraulics as joint actuation or need machine-specific data, tuning or simulation. They do not treat LS and NFC machines in a unified way. Model-free RL can be robust, but has not shown centimeter-level accuracy in deep heavy-duty grading. None of these works provides a short retrofit calibration procedure for hydraulic adaptation across excavators.

C. Grading and Surface Flattening

Several works address grading and surface flattening with hydraulic excavators. Xu et al. [31] proposed an automated grading controller based on Inverse Kinematics and PI hydraulic control. Coupling the PI controllers can lead to improved precision as shown by Wang et al. [26]. Lee et al. [17] formulated contour control for leveling tasks based on geometric path-following of the bucket edge by decoupling the target surface objective from pure position control. More recent work uses contouring-error formulations and disturbance observers to achieve high-accuracy flattening: Dao et al. [5] presents contouring control for surface flattening and later extends the approach with active disturbance rejection and sliding-mode observation to better cope with external disturbances and model mismatch [4]. These techniques are evaluated in simulation only. Yang et al. [32] present a leveling controller for hydraulic excavators that combines a force pre-load term with cross-coupling compensation to synchronize cylinder motions on a small LS excavator.

Commercial solutions such as Trimble Earthworks and earlier GCS900 systems provide GNSS- and total-station-based guidance and semi-automatic boom, stick, and bucket control

TABLE I
COMPARISON TO PRIOR GRADING AND HYDRAULIC MOTION-CONTROL METHODS.

Ref.	**Technology**	**Val.**	**Performance**	**Machine specificity**	**Arch.**
[31]	IK + PI	Sim.	~4 cm in sim, slow	single-machine model	simplified
[5]	Contouring + ESO	Sim.	N/A	simulation-only	not considered
[4]	ADRC + SMO contouring	Sim.	N/A	simulation-only	not considered
[16]	Hybrid model-based + RL	Sim.	2.3 cm	tuned one simulated 30 t excavator	in-air LS
[32]	Force preload + cross-coupling	Real	light grad. only: 1 cm	tuned on 6 t LS excavator	LS
[26]	Coupled non-linear PI	Real	in-air only: ~2–9 cm	tuned on one machine	N/A
[17]	Contour following + PI	Real	light grad. only: 2.34 cm avg	tuned on 1.5 t machine	N/A
[18]	Learned model inversion	Real	< 2 cm path RMSE	several hours of machine-specific data	unclear
[21]	Data-driven nonlinear MPC	Real	cyl vel tracking only	identified on one excavator	LS
[11, 3, 9]	Commercial, Proprietary	Real	> 4 cm or light grading only	retrofittable	various
Ours	**Hydraulic FF + PID + MPC**	**Real**	**1.4 / 1.8 cm RMSE**	**~20 min, explicit calibration**	**LS + NFC**

Val.: validation type. *Arch.*: whether the method explicitly addresses hydraulic architectures. N/A: not available in public description.

for excavator grading [11]. Caterpillar's Cat Grade Control offers assistive modes to reach design surfaces and slopes and is tightly integrated with machine telematics and payload systems [3]. Leica's MC1 platform provides 2D machine control for multiple earthmoving machines, including excavators, and focuses on unified user interfaces and integration with survey equipment [9]. Details of the hydraulic control strategies and their adaptation to different hydraulic architectures are typically not disclosed in public documentation. However, as construction robotics is a more mature field, commercial solutions tend to match the performance of what is presented in literature. Empirically, these systems perform well in light grading and finishing, but are limited in deeply loaded cuts and their use of the full hydraulic torque envelope.

All methods operate mainly in the kinematic or joint-velocity domain. They generally assume relatively light terrain interaction, do not explicitly model hydraulic dynamics or load-dependent effects, and ignore differences in joint response to input commands. In contrast, our controller is retrofittable, hydraulics-aware, and machine-agnostic for heavy-duty high-precision grading.

Table I compares previous methods by validation type, performance, machine specificity, and hydraulic handling used. Because many prior methods require vendor-level access, large datasets, extensive tuning, tuned simulation, or assumptions that do not hold on both excavators, we use a transferable commercial system deployed on the same machine as the practical baseline. To the best of our knowledge, no prior method combines real in-soil validation, sub-2 cm RMSE, short calibration, cross-machine deployment, and explicit handling of soft NFC actuation.

III. CONTROLLER ARCHITECTURE

The presented controller executes a single grading pass in the soil until the end of travel is reached or the machine stalls at maximum function pressure. Our control pipeline receives as input from the user or a higher-level planner the height and inclination of the design surface, along with the desired grading velocity in end-effector (EE) space. To keep the motion controller adaptable across different machine types,

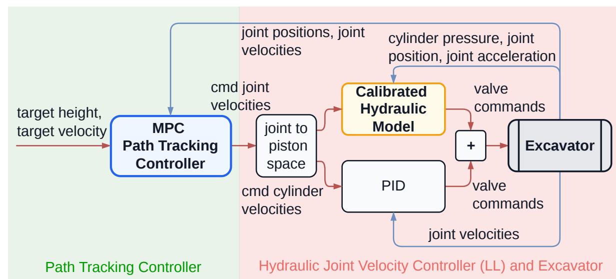

Fig. 2. Flow graph of the grading controller and split between path tracking and joint velocity stage. The user sets the design surface and EE speed. The MPC path-tracking controller outputs joint velocities, which are tracked by the hydraulic controller consisting of a hydraulic model and a parallel PID element.

we separate machine-agnostic path tracking from hydraulics-aware joint velocity control, as shown in Figure 2.

A. Joint Velocity Controller

Our core innovation includes a hydraulic-aware joint velocity controller that tracks target joint rates by computing a valve command or pilot-stage current. Since joint-level effects occur at the cylinder level and are more linear there, we map the target joint rates [rad/s] to cylinder speeds [$\mathrm{m\,s^{-1}}$] via the closed-loop kinematics of each joint, as shown by Werner et al. [30]. The target cylinder velocity is then fed to a calibrated hydraulic model as a Feed Forward (FF) element and to a parallel PID controller. During calibration, an appropriate hydraulic model is selected, enabling our method to generalize across hydraulic control loops such as LS and NFC. Different hydraulic architectures vary significantly in their response to joint loading, making this adaptation vital. The PID controller compensates for unmodeled effects and disturbances, such as flow sharing, pump boost, or recuperation, while most of the command comes from the calibrated, load-aware hydraulic FF model. While cross-coupling effects are present on all architectures, we found them to be compensatable with just the PID for our target speed and precision. Implemented as a multidimensional Lookup Table (LUT), our hydraulic model maps desired cylinder velocities or function flows to valve commands using other measurements such as cylinder back pressure and joint acceleration. It acts as a Multiple Input Single Output (MISO) element and is calibrated for each joint individually. Finally, the FF and PID signals are combined and sent to the valves.

1) Hydraulic Model Load Sensing: Due to the load-aware and compensating behavior of LS hydraulics, the calibrated hydraulic model can be designed in a straightforward way. A 1:1 LUT, mapping from desired oil flow to valve command, calibrated on the machine as described in Section IV-A is sufficient. Appendix A-A explains the hydraulic mechanisms behind this model.

2) Hydraulic Model NFC: NFC hydraulics differ from LS in how function loading affects motion [19]. Appendix A-B describes the more complex relationship between function load and flow in NFC systems. It also describes the underlying hydraulic model, that we calibrate as shown in Section IV-B for the hydraulic-aware feed-forward element in our load-sensitive controller. The simplified model is our key contribution, as it lets us calibrate and model NFC hydraulics with a task-specific goal. Hydraulic modeling is otherwise practically unviable for researchers due to the unavailability of core information from manufacturers and the difficulty of characterizing individual components, which requires full disassembly.

B. Path Tracking Controller

Our path tracking controller uses the machine kinematics and transient behavior of the plant, which includes our joint velocity controller and the machine itself. A standard MPC formulation is deployed, which uses a per-joint second-order transfer function with added dead-time delay as a system model. By accounting for joint transients, the MPC path tracking controller commands joint velocities that avoid the typical overshoot of the target surface at the start of a grading pass. We neglect joint coupling effects in favor of execution time, since they have shown limited influence on joint dynamics at the speeds targeted by this work. Future work could include them by explicitly modeling them in the MPC formulation.

The MPC's objective is to execute a single grading pass along the design surface while respecting joint and actuator limits, outputting target joint rates for the joint velocity controller. As an input, it gets the design surface height $h^\star$, inclination $\alpha^\star$ and EE velocity $v_x^\star$. The controller is formulated as a discrete-time nonlinear MPC in joint space with a task-space tracking objective, where the EE pose and twist are predicted through forward kinematics.

a) Prediction model.: The MPC state models the dominant closed-loop transient of each joint, including the calibrated hydraulic feedforward element, PID velocity loop and hydro-mechanical motion of the machine. Each joint i is approximated as a second-order system in velocity with gain K_i, damping ratio ζ_i, natural frequency $\omega_{n,i}$, acceleration a_i and dead time τ_i acting on the commanded joint velocity u_i at time t:

$$\dot{a}_i = -2\zeta_i\omega_{n,i}\, a_i - \omega_{n,i}^2\, v_i + K_i\omega_{n,i}^2\, u_i(t-\tau_i), \tag{1}$$

with $v_i = \dot{\theta}_i$ and $a_i = \ddot{\theta}_i$. For the controlled joints, we define joint positions $\boldsymbol{\theta} \in \mathbb{R}^3$, velocities $\dot{\boldsymbol{\theta}} \in \mathbb{R}^3$, and accelerations $\ddot{\boldsymbol{\theta}} \in \mathbb{R}^3$. The control input is the commanded joint velocity $\boldsymbol{u} = \dot{\boldsymbol{\theta}}_{\text{cmd}} \in \mathbb{R}^3$. The model is discretized at $\Delta t = 0.1\,\text{s}$, matching the controller update rate.

Dead time is represented using a discrete input buffer of length N_d that is part of the MPC state. Let $\boldsymbol{u}_{d,j} \in \mathbb{R}^3$ denote the j-th delayed-input state, with $j = 1$ the most recent, and $(\cdot)^+$ denoting the next-step value. The buffer dynamics are

$$\boldsymbol{u}_{d,1}^+ = \boldsymbol{u}, \qquad \boldsymbol{u}_{d,j}^+ = \boldsymbol{u}_{d,j-1}, \qquad j = 2,\dots,N_d. \tag{2}$$

For joint i, the delayed input used in (1) is selected as $u_i(t-\tau_i) \approx (\boldsymbol{u}_{d,d_i})_i$ with

$$d_i = \operatorname{clip}\left(\left\lfloor \frac{\tau_i}{\Delta t} \right\rfloor,\, 1,\, N_d\right), \tag{3}$$

where $\lfloor\cdot\rfloor$ is the floor operator and $\operatorname{clip}(\cdot, 1, N_d)$ saturates the value to the interval $[1, N_d]$.

b) Task-space quantities.: The MPC cost is defined in task space. The excavator forward kinematics are evaluated inside the optimization using the predicted joint states. Specifically, the full configuration used for kinematics is

$$\boldsymbol{q}_{\text{full}} = \begin{bmatrix}\theta_{\text{cab}} & \theta_{\text{boom}} & \theta_{\text{stick}} & \theta_{\text{bucket}}\end{bmatrix}^\top, \tag{4}$$

where θ_{cab} is the measured cabin pitch. For machines with a telescopic stick, stick extension measurements ℓ_{tele} can be added to the state. From $\boldsymbol{q}_{\text{full}}$ and $\dot{\boldsymbol{q}}_{\text{full}}$ we obtain the predicted EE state $\boldsymbol{\pi}$ including position $\boldsymbol{p}_{\text{EE}}(\cdot)$, EE linear velocity $\boldsymbol{v}_{\text{EE}}(\cdot)$, and EE angular velocity $\boldsymbol{\omega}_{\text{EE}}(\cdot)$, all expressed in a local gravity-aligned frame. The bucket pitch angle ϕ_{EE} is extracted from the predicted EE rotation matrix.

c) Optimization problem and cost function.: At each control step, the MPC solves a finite-horizon nonlinear program in receding-horizon fashion:

$$\min_{\{\boldsymbol{u}_k\}_{k=0}^{N-1}} \quad \sum_{k=0}^{N-1} \ell(\boldsymbol{x}_k, \boldsymbol{u}_k, \boldsymbol{\pi}_k) + m(\boldsymbol{x}_N, \boldsymbol{\pi}_N) \tag{5}$$

$$\text{s.t.} \quad \boldsymbol{x}_{k+1} = f(\boldsymbol{x}_k, \boldsymbol{u}_k, \boldsymbol{\pi}_k), \tag{6}$$

$$\boldsymbol{x}_0 = \hat{\boldsymbol{x}}(t), \qquad \boldsymbol{u}_k \in \mathcal{U}, \qquad \boldsymbol{\theta}_k \in \Theta. \tag{7}$$

Here, $\boldsymbol{x}_k$ is the MPC state at step k (containing the joint states and the delayed-input buffer), and $\hat{\boldsymbol{x}}(t)$ is the estimated current state at time t. The mapping $f(\cdot)$ denotes the (discretized) state-transition function induced by (1) and the delay-buffer dynamics (2). The stage cost $\ell(\cdot)$ and terminal cost $m(\cdot)$ are scalar-valued functions. The admissible input set $\mathcal{U}$ encodes joint-rate limits, and the admissible set Θ encodes joint-position limits.

For slope grading, the running cost penalizes deviation from the desired forward velocity, enforces near-zero vertical EE velocity and pitch rate, regulates the EE height to the target plane, and regulates the blade pitch:

$$\begin{aligned}\ell(\boldsymbol{x}_k, \boldsymbol{u}_k, \boldsymbol{\pi}_k) = {} & w_{vx} \left(v_{\mathrm{EE},x}(\boldsymbol{x}_k) - v_x^\star\right)^2 \\ & + w_{vz} \left(v_{\mathrm{EE},z}(\boldsymbol{x}_k) - 0\right)^2 \\ & + w_{\omega} \left(\omega_{\mathrm{EE},y}(\boldsymbol{x}_k) - 0\right)^2 \\ & + w_{\phi} \left(\phi_{\mathrm{EE}}(\boldsymbol{x}_k) - \phi^\star\right)^2 \\ & + w_h \left(p_{\mathrm{EE},z}(\boldsymbol{x}_k) - (h^\star + \alpha^\star p_{\mathrm{EE},x}(\boldsymbol{x}_k))\right)^2 \\ & + w_{\Delta u} \left\|\boldsymbol{u}_k - \boldsymbol{u}_{k-1}\right\|_2^2 .\end{aligned}$$

The increment penalty on $\boldsymbol{u}_k - \boldsymbol{u}_{k-1}$ promotes smooth joint velocity commands and reduces excitation of unmodeled effects in the low-level hydraulic loop. The terminal cost focuses on converging to the target height,

$$m(\boldsymbol{x}_N, \boldsymbol{\pi}_N) = w_{h,N} \left(p_{\mathrm{EE},z}(\boldsymbol{x}_N) - \left(h^\star + \alpha^\star p_{\mathrm{EE},x}(\boldsymbol{x}_N)\right)\right)^2 . \tag{8}$$

In the implementation, w_ϕ is set to zero when the bucket joint is disabled.

d) Constraints.: We enforce actuator and joint limits through the constraint sets $\mathcal{U}$ and Θ.

$$\boldsymbol{u}_{\min} \leq \boldsymbol{u}_k \leq \boldsymbol{u}_{\max}, \quad \boldsymbol{\theta}_{\min} \leq \boldsymbol{\theta}_k \leq \boldsymbol{\theta}_{\max}. \tag{9}$$

When bucket motion is disabled, we tighten the bounds at each step to the current measured value and constrain the bucket velocity, acceleration, and input to zero. This preserves a fixed state dimension while enforcing the desired reduced actuation.

e) Real-time implementation.: The MPC is solved at 10 Hz with horizon length $N = 20$. The solver receives the current joint state estimate $\hat{\boldsymbol{x}}(t)$ and the delayed input buffer from the previously applied commands. The commanded task-space velocity $\boldsymbol{v}^\star$ is treated as a time-varying parameter and updated at each step. In MPC fashion, only the first control input is executed in each tick.

IV. Calibration

This section describes the calibration of all free parameters in the controller pipeline, which is our second major contribution. Our calibration procedure takes about 20 min and requires no disassembly of the system. Each joint is calibrated sequentially and in isolation, since coupling effects are not included in the model, starting with the joint velocity controller and finishing with the path tracking controller. For the joint velocity controller, we calibrate our hydraulic FF model as a LUT. Lookup values are directly sampled on LS machines and derived from our variable displacement pump- and function orifice model on NFC hydraulics according to Section III-A2 and detailed in A-B. After calibrating the hydraulic FF model (Sections IV-A and IV-B), the PID controller is tuned using standard methods [34]. For the path-tracking controller, we identify the transient response of the plant, containing the FF element, PID controller, and hydraulic system.

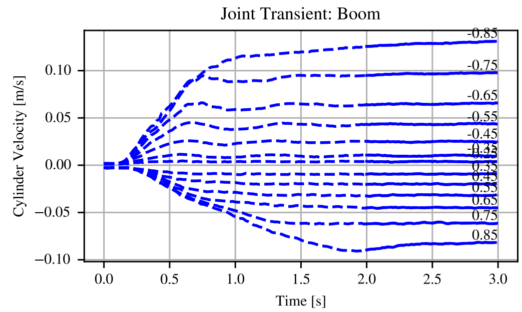

Fig. 3. FF data collection for the Boom joint. Normalized commands from -0.85 to 0.85 in steps of 0.1 with the resulting joint velocity response and steady-state part shown as a solid line. Data from Menzi Muck M445.

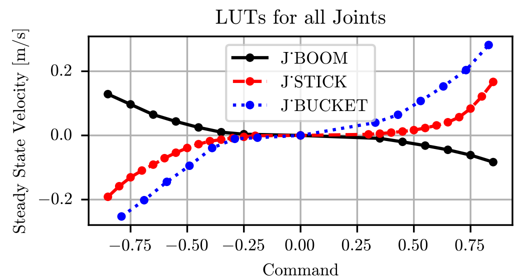

Fig. 4. Hydraulic FF model of the LS M445. LS enables a direct mapping between cylinder velocity and command.

In order to perform the calibration in the more linear cylinder space, we convert between cylinder and joint space using the position-dependent sensitivity factor $\gamma(\boldsymbol{\Theta})$. It maps cylinder forces $\mathbf{f}$ to joint torques $\boldsymbol{\tau}$ and cylinder velocities $\mathbf{v}$ to joint rates $\dot{\boldsymbol{\Theta}}$. The measured cylinder force $\mathbf{f_m}$ is computed from pressure readings on the a and b sides together with the corresponding plunger areas, as shown in Equation (10) for one cylinder.

$$f_m = p_a A_a - p_b A_b \tag{10}$$

A. Load Sensing

As LS hydraulics show no significant load-dependent behavior, calibration reduces to the mapping from valve command u to cylinder velocity v. We collect a dataset that spans the operational range of valve commands with small increments. Figure 3 shows the measured cylinder responses for normalized commands in $[-0.85, \ldots, 0.85]$. The average velocity over the third second after applying the command is used as the steady-state value. We then apply linear interpolation between sampled velocities v to obtain the final lookup function, as shown in Figure 4.

B. Negative Flow Control

We propose a novel procedure for calibrating the FF element in NFC hydraulics, taking the load-dependent behavior into consideration. Our method outputs a 2D LUT that maps the desired cylinder speed and the current cylinder force to a

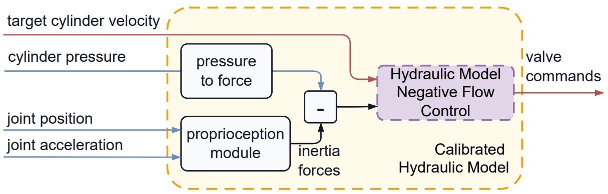

Fig. 5. Flow chart of the FF element for NFC hydraulics. Inertia compensation for removal of system torques.

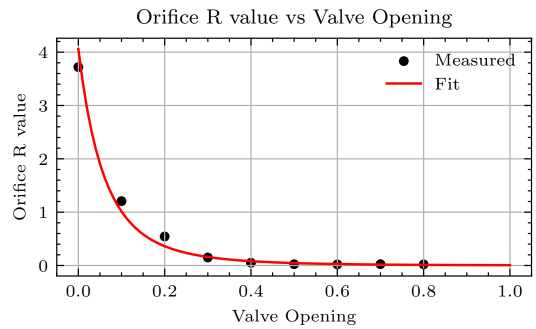

Fig. 6. Identified orifice function for Stick. It maps hydraulic resistance to the valve command.

valve command. Since it is not feasible to excite a fine grid of all speed and load combinations for direct calibration, we derive the LUT from our simplified hydraulic model in Section III-A2, A-B, thus enabling straightforward calibration of NFC hydraulics. We identify the dependence of valve command on pump pressure and the free parameters of the function orifice in the DCV.

1) Inertia Compensation: The pressure-derived cylinder force includes internal system forces and external forces from shovel–ground interaction. System forces depend on joint position (gravity), velocity (friction), and acceleration (inertia). Gravity and friction create a quasi-static load, that is therefore compensated for by the FF element. On the other hand, inertia-induced forces can create a positive feedback loop: a higher valve command increases acceleration, which causes a spike in reaction cylinder force, which then leads the FF element to command an even higher valve command in order to compensate for the perceived increase in momentary load. This can make transients highly unstable. We therefore estimate the inertia forces at the cylinder as described by Werner et al. [30] and use inertia-compensated forces for the NFC FF element as shown in Figure 5.

2) Hydraulic Model: From the inertia-compensated cylinder forces, we compute an artificial cylinder back pressure at the function line as in Equation (11), where $A_{\text{articulation}}$ is the effective area of the active cylinder side in the calibrated direction. Since external loading may act opposite to the articulation, the resulting function pseudo back pressure P_f can also be negative.

$$P_f = (f_m - f_{\text{inertia}})/A_{\text{articulation}} \tag{11}$$

We model the pump's pressure loop setpoint with respect to the DCV command x as a LUT with linear interpolation $P_p(x)$. Furthermore, we calibrate the relationship between valve command x and hydraulic resistance of the variable in-line orifice of the DCV, represented by R_3 in A-B. The resistance of the variable orifice in the DCV is modeled by Equation (12),

$$R(x) = \frac{a}{b \cdot (x+c)^2} \tag{12}$$

where the free parameters a, b and c are fitted from measurements of the volume flow into the function Q_{func} and the function-side pseudo back pressure P_f. The pressure over R_3 is then given by $P = P_p(x) - P_f$. The orifice resistance R is a lumped parameter derived from the turbulent orifice equation (13), which is simplified to (14).

$$\Delta P = \frac{Q^2 \rho}{2 C_d^2 A^2} \tag{13}$$

$$\Delta P = R \cdot Q^2 \tag{14}$$

In practice, identification of R requires a dataset with different joint loadings for the same valve command x.

a) Stick, Bucket: For the `Stick` and `Bucket` joints we command a constant valve opening and progressively stall the bucket in the ground until standstill, which increases the joint load. This motion generates trajectories of increasing P_f and decreasing Q_f that we use to fit the parameter $R_{\text{test},x}$ for each test command x.

b) Boom: Since for the lifting direction of the `Boom` joint progressive stalling is not feasible, we record trajectories with different joint loads at the same command. The configurations curled, erected, and erected with a full bucket are sufficient for calibration. Each configuration yields one data point that we use in the same way as the trajectories of the previous joints.

3) Lookup Table: We fit Equation (12) to the experimentally determined $R_{\text{test},x}$ values with a logarithmic cost to preserve precision for small R as shown in Equation (15).

$$\min_{a,b,c} \sum_{x \in x_{\text{test}}} \left[\left| \log(R(x)) - \log(R_{\text{test},x}) \right| \right] \tag{15}$$

The identified orifice model $R(x)$ shown in Figure 6 and pump model $P_p(x)$ are inverted to form a two-dimensional LUT that maps desired flow and current pseudo back pressure P_f to a valve command x. This table is the hydraulic model for a negative flow control function and is shown in Figure 7.

C. MPC Model

The MPC controller is independent of the hydraulic model and assumes a stiff low-level controller, where small commands reach maximum function pressure at stall. We calibrate the joint model from step responses with dead-time τ, scalar K, damping ζ and natural frequency ω of the combined PID, hydraulic model and plant as shown in Figure 8.

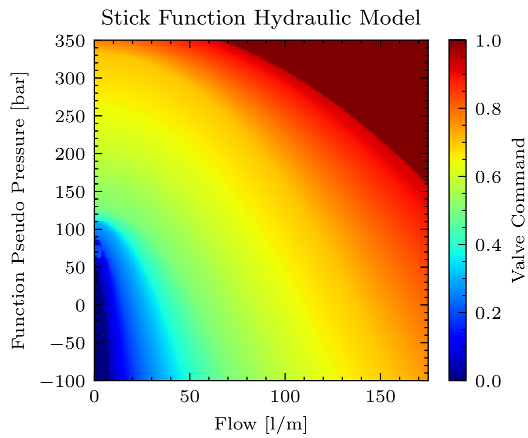

Fig. 7. Hydraulic model for the Stick function on CASE250. Load-dependent mapping from valve command to flow (cylinder speed).

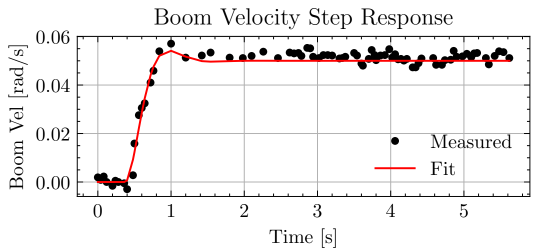

Fig. 8. CASE250 Boom step response identification with a commanded joint rate of 0.05 rad/sec.

V. Experiments

The presented method was tested and evaluated on a 11.5 t LS excavator: Menzi Muck M445, and on a 25 t NFC standard machine: CASE250. The first experiments test hydraulic model accuracy under load. The core quantitative evaluation is in-soil path tracking on CASE250 and M445 across cutting depths and external soil loads, including high-load passes near stall. A separate CASE250 surface-finish test measures final terrain quality against a commercial system. Preliminary analysis showed that the machine-specific commercial controller matches a straightforward PID+IK controller for grading.

A. Hydraulic FF

To validate the hydraulic FF model, we benchmark the joint velocity tracking performance of the FF element for different payloads and thus joint loadings. On the LS M445 this experiment only validates the calibrated LUT, since the system reacts stiff to different loads. A joint-velocity tracking accuracy of $\approx$ 2% is achieved, confirming the LS model and calibration. On the CASE250 this experiment shows that the hydraulic model can compensate for the load-dependent joint dynamics. Figure 9 shows a `Boom` lifting command of 0.05 rad s^{-1} for three payload scenarios. The target joint velocity is accurately tracked by the load-dependent FF term, including changing gravity loading during the lift, as visible in the FF output. Comparable performance is obtained over the full machine velocity range and payloads.

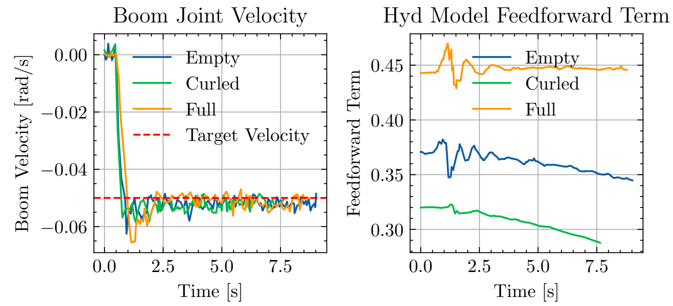

Fig. 9. Contribution of calibrated NFC hydraulics FF model. PID controller disabled. The pressure-dependent FF term achieves the target joint velocity independent of the joint loading.

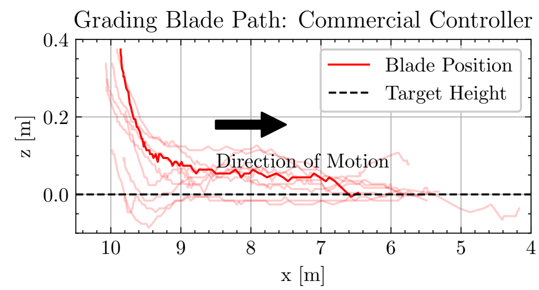

Fig. 10. CASE250, Commercial Controller: Evaluation of 10 grading passes of varying depth in compacted soil. RMSE: 4.7 cm (9 m and closer)

B. Grading

Our grading experiments test the full stack, including joint velocity control and MPC path tracking. We compare the precision of the proposed system with a commercially available semi-automatic grading controller and evaluate our proprioceptive path-tracking accuracy and soil-planing accuracy across multiple passes using a laser scanner. All experiments, including those with the commercial system, use a blade velocity of approximately 0.5 m s^{-1} for comparability. This velocity is close to that of an expert operator during fine grading, who removes less material but achieves similar surface accuracy.

1) Path Tracking: We collect trajectories from light surface grading to deeper cuts, high-load passes, and near-stall cuts in compacted material from 2 cm to 40 cm deep. The deep paths in Figures 10–12 fill the bucket in less than one stroke. We also test whether the machine reaches maximum torque and whether the blade is pushed away from the target surface.

a) Commercial (CASE250): Figure 10 shows the trajectory tracking of the commercial controller on the CASE250. After the first meter of approach to the target, it tracks with an **RMSE of 4.7 cm** and a maximum **path deviation of 17 cm** (9 m and closer). In hard soil the controller does not reach the target depth, while in light soil a substantial initial overshoot is visible. Many trajectories stall before the end of travel at about 5 m with stick pressures far below the maximum function pressure of 350 bar. In some hard soil conditions the shovel is pushed up at the end of travel, reducing accuracy close to the machine.

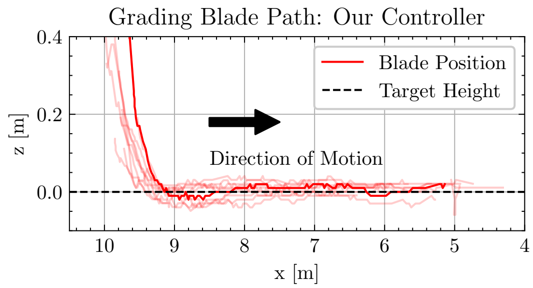

Fig. 11. CASE250, Our Controller: Evaluation of 10 grading passes of varying depth in compacted soil. RMSE: 1.8 cm (9 m and closer)

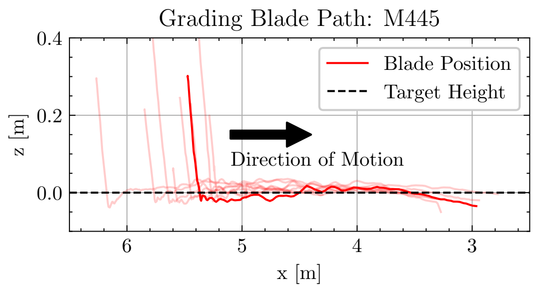

Fig. 12. M445, Our Controller: Evaluation of 10 grading passes of varying depth in compacted soil. RMSE: 1.4 cm (5.2 m and closer). Varying starting distances are a result of different extensions of the telescopic stick on M445.

b) *Ours (CASE250):* As shown in Figure 11, the presented controller achieves an **RMSE of 1.8 cm** and a maximum **path deviation of 5 cm** on the same machine and conditions. It maintains high accuracy regardless of soil conditions and reliably reaches the target height after about one meter of approach. Light grading passes show no initial overshoot, and in most cases the end of travel is reached. When the machine stalls earlier, the stick pressure reaches the maximum function pressure of the machine.

c) *Ours (M445):* Figure 12 shows our controller on the LS Menzi Muck M445 with an **RMSE of 1.4 cm**[1] and a maximum **path deviation of 4 cm**. On M445 the trajectories start at different distances due to the variable reach from the telescopic joint which is initialized at different lengths but kept fixed during episodes. No loss of precision from varying cutting depths is visible, consistent with the CASE250 results. The trajectory stalls at maximum function pressure and shows no significant initial overshoot.

2) *Surface Quality:* This separate CASE250 test evaluates final surface finish, not path tracking, as seen in Figure 13. The test is performed on compacted sand with a cutting depth of about 25 cm. The target area is four shovel widths wide and graded from left to right, one pass per lateral position with about 20% overlap (five passes total) to avoid spillage. Surface quality is measured by laser scan with a Leica MS60 Multistation. Figure 14 shows the two graded areas side by side, with color indicating deviation from the target surface and gray points outside the graded area. The commercial controller does not reach the target height until the midpoint

[1]Much lower in-air. Precise enough to open a bottle. Check our supplementary video for a visual demonstration of the achieved accuracy.

Fig. 13. Experiment Setup for Surface Quality Measurements on CASE250. Fixed Leica MS60 scan used for evaluation of the surface quality.

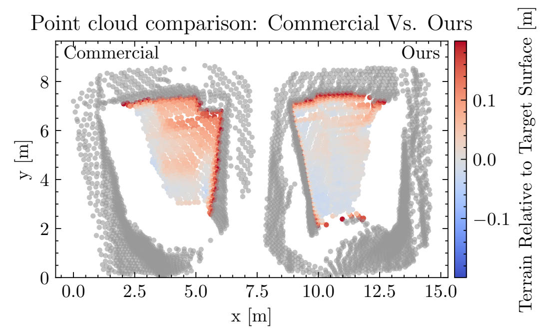

Fig. 14. CASE250: Comparison of the two graded surfaces: target surface was not reached with the commercial system, higher precision and consistency from our method. Gray points are outside of the testing area and included for context, white areas are shadowed in the scan.

of the pass and shows large deviations and surface oscillations with magnitudes larger than 10 cm. The presented controller reaches the target surface earlier, creates a flatter surface at the target height and does not oscillate.

C. Discussion

Our calibrated hydraulic FF terms track joint velocity commands across payloads on LS and NFC machines. Grading experiments show that the proposed controller reaches the target surface after about one meter and maintains low deviation in compacted material up to 40 cm cutting depth. Our setup **outperforms the commercial controller by a factor of 2.6** (RMSE 1.8 cm vs. 4.7 cm) and avoids premature stalling by using maximum function pressure. Laser scans confirm a flatter surface with fewer oscillations and earlier convergence to the target height.

Our once-per-machine retrofitting process of the presented controller can adapt to LS and NFC hydraulic machines. It starts with the identification and tuning of the hydraulic-specific low-level controller, which includes inertia compensation for NFC machines. The transfer functions of the plant including machine and low-level controller are then identified and updated in the MPC EE space controller. The whole process takes about 20 min.

VI. Future Work, Limitations, and Conclusion

A. Future Work and Limitations

Future work will address tracking arbitrary shapes via a more expressive cost function and will include end-effector forces in Cartesian space in the MPC objective to enable impedance-style control for proprioceptive compaction and redistribution of piles. Limitations of this work are the applicability of our method to Positive Flow Control machines, which has not been evaluated, as no machine with this architecture was available to the authors. The hydraulic model can be extended to capture coupling effects between functions, enabling faster motions at higher precision.

B. Conclusion

This work presents a retrofittable, machine-agnostic control stack for high-precision, heavy-duty grading with hydraulic excavators. Our joint velocity controller targets multiple hydraulic architectures, including LS, and for NFC machines we formulate a novel load-aware model. Furthermore, we formulate a practical calibration procedure that targets field deployment: it relies only on kinematic parameters and onboard sensing and runs in about 20 min. Experiments on a 11.5 t LS and a 25 t NFC excavator validate the FF joint velocity accuracy and in-soil grading performance of the combined system. Our system executes grading passes in compacted material with cutting depths up to 40 cm, respects actuator limits, and preserves smooth joint commands through explicit transient and dead-time modeling. In heavy-duty grading trials, the proposed controller outperforms a state-of-the-art commercially available semi-automatic system on the same NFC excavator and uses the full torque potential. Overall, the proposed retrofittable controller achieves centimeter-level grading at 2.6 times better accuracy in compacted material and generalizes across common hydraulic architectures. Adoption of our grading framework can reduce the number of autonomous passes required in earthworks, resulting in substantial cost reductions.

Acknowledgments

This project received funding from Hexagon AB and was supported by the Swiss National Science Foundation through the National Centre of Competence in Digital Fabrication (NCCR dfab).

References

[1] Koji Aoshima and Martin Servin. Examining the simulation-to-reality gap of a wheel loader digging in deformable terrain. *Multibody System Dynamics*, July 2024. ISSN 1573-272X. doi: 10.1007/s11044-024-10005-5.

[2] Ehsan Rezazadeh Azar and Vineet R Kamat. Earthmoving equipment automation: a review of technical advances and future outlook. *Tcon*, 22:247–265. URL https://www.itcon.org/2017/13.

[3] Caterpillar. Cat grade for excavators. https://www.cat.com/en_US/products/new/technology/grade/grade/15969804.html. Accessed: 2025-11-10.

[4] Hoang Vu Dao and Kyoung Kwan Ahn. Active Disturbance Rejection Contouring Control of Robotic Excavators with Output Constraints and Sliding Mode Observer. *Applied Sciences*, 12(15):7453, 2022. ISSN 2076-3417. doi: 10.3390/app12157453.

[5] Hoang Vu Dao, Seonjun Na, Duc Giap Nguyen, and Kyoung Kwan Ahn. High accuracy contouring control of an excavator for surface flattening tasks based on extended state observer and task coordinate frame approach. *Automation in Construction*, 130:103845, October 2021. ISSN 0926-5805. doi: 10.1016/j.autcon.2021.103845.

[6] Timothy W. Dell, editor. *Hydraulic Systems for Mobile Equipment*. G-W Publisher, 2023.

[7] Pascal Egli and Marco Hutter. A General Approach for the Automation of Hydraulic Excavator Arms Using Reinforcement Learning. *IEEE Robotics and Automation Letters*, 7(2):5679–5686, April 2022. ISSN 2377-3766. doi: 10.1109/LRA.2022.3152865.

[8] Pascal Egli, Lorenzo Terenzi, and Marco Hutter. Reinforcement Learning-Based Bucket Filling for Autonomous Excavation. *IEEE Transactions on Field Robotics*, 1:170–191, 2024. doi: 10.1109/TFR.2024.3432508.

[9] Leica Geosystems. Leica mc1. https://leica-geosystems.com/en-us/products/machine-control-systems/software/leica-mc1. Accessed: 2025-11-10.

[10] Jonas Gruetter, Lorenzo Terenzi, Pascal Egli, and Marco Hutter. Towards Learning Boulder Excavation with Hydraulic Excavators. 2025. doi: 10.48550/arXiv.2509.17683.

[11] Trimble Inc. Trimble earthworks. https://heavyindustry.trimble.com/en/products/grade-control-excavators. Accessed: 2025-11-10.

[12] Inkyu Jang, Junha Kim, Dongjae Lee, Changhyeon Kim, Changsuk Oh, Youngbum Kim, Sangwook Woo, Heejee Sung, and H. Jin Kim. Towards Fully Integrated Autonomous Excavation: Autonomous Excavator for Precise Earth Cutting and Onboard Landscape Inspection. *IEEE Robotics & Automation Magazine*, 32(3):88–102, 2025. doi: 10.1109/MRA.2024.3400772.

[13] Shiyu Jin, Zhixian Ye, and Liangjun Zhang. Learning Excavation of Rigid Objects with Offline Reinforcement Learning. 2023. doi: 10.48550/arXiv.2303.16427.

[14] Dominic Jud, Philipp Leemann, Simon Kerscher, and Marco Hutter. Autonomous Free-Form Trenching Using a Walking Excavator. *IEEE Robotics and Automation Letters*, 4(4):3208–3215, 2019. doi: 10.1109/LRA.2019.2925758.

[15] Kwangmin Kim, Minji Kim, Dongmok Kim, and Dongjun Lee. Modeling and velocity-field control of autonomous excavator with main control valve. *Automatica*, 104:67–81, 2019. ISSN 0005-1098. doi: 10.1016/j.automatica.2019.02.041.

[16] Youngbum Kim and Jinwhan Kim. Enhanced Hydraulic Excavator Control via Semi-automatic Grading Control Using Reinforcement Learning. *International Journal of Control, Automation and Systems*, 23(3):896–906, 2025. ISSN 2005-4092. doi: 10.1007/s12555-024-0213-9.

[17] Chang Seop Lee, Jangho Bae, and Daehie Hong. Contour

control for leveling work with robotic excavator. *International Journal of Precision Engineering and Manufacturing*, 14(12):2055–2060, December 2013. ISSN 2005-4602. doi: 10.1007/s12541-013-0278-5.

[18] Minhyeong Lee, Hyelim Choi, ChangU Kim, Jihyun Moon, Dongmok Kim, and Dongjun Lee. Precision Motion Control of Robotized Industrial Hydraulic Excavators via Data-Driven Model Inversion. *IEEE Robotics and Automation Letters*, 7(2):1912–1919, April 2022. ISSN 2377-3766. doi: 10.1109/LRA.2022.3142389.

[19] Ruichuan Li, Qiyou Sun, Xinkai Ding, Yisheng Zhang, Wentao Yuan, and Tong Wu. Review of Flow-Matching Technology for Hydraulic Systems. *Processes*, 10(12): 2482, December 2022. ISSN 2227-9717. doi: 10.3390/pr10122482.

[20] Qingkai Lu, Yifan Zhu, and Liangjun Zhang. Excavation Reinforcement Learning Using Geometric Representation. *IEEE Robotics and Automation Letters*, 7 (2):4472–4479, April 2022. ISSN 2377-3766. doi: 10.1109/LRA.2022.3150511.

[21] Salim Msaad, Leonardo Cecchin, Ozan Demir, and Lorenzo Fagiano. Data-Driven Model Predictive Control of an Hydraulic Excavator via Local Model Networks. In *2025 American Control Conference (ACC)*, page 85–90, 2025. doi: 10.23919/ACC63710.2025.11107493.

[22] Huynh A. D. Nguyen and Quang P. Ha. Robotic autonomous systems for earthmoving equipment operating in volatile conditions and teaming capacity: a survey. *Robotica*, 41(2):486–510, February 2023. ISSN 0263-5747, 1469-8668. doi: 10.1017/S0263574722000339.

[23] Filippo A. Spinelli, Pascal Egli, Julian Nubert, Fang Nan, Thilo Bleumer, Patrick Goegler, Stephan Brockes, Ferdinand Hofmann, and Marco Hutter. Reinforcement Learning Control for Autonomous Hydraulic Material Handling Machines with Underactuated Tools. *International Conference on Intelligent Robots and Systems*, page 12694–12701, October 2024. ISSN 2153-0866. doi: 10.1109/IROS58592.2024.10802199.

[24] Sergiy Sydorenko. Negative flow control vs load sensing - which one is better? https://www.insanehydraulics.com /letstalk/nfcvsls.html, 2025. Accessed: 2025-12-04.

[25] Lorenzo Terenzi and Marco Hutter. Toward Autonomous Excavation Planning. *IEEE Transactions on Field Robotics*, 1:292–317, 2024. ISSN 2997-1101. doi: 10.1109/TFR.2024.3485037.

[26] Dongyun Wang, Lijuan Zheng, Hongxiang Yu, Wu Zhou, and Liping Shao. Robotic excavator motion control using a nonlinear proportional-integral controller and cross-coupled pre-compensation. *Automation in Construction*, 64:1–6, April 2016. ISSN 09265805. doi: 10.1016/j.autcon.2015.12.024.

[27] Jian Wang, Hao Zhang, Peng Hao, and Hua Deng. Observer-Based Approximate Affine Nonlinear Model Predictive Controller for Hydraulic Robotic Excavators with Constraints. *Processes*, 11(7), 2023. ISSN 2227-9717. doi: 10.3390/pr11071918. Multidisciplinary Digital Publishing Institute.

[28] Tao Wang and Qingfeng Wang. Efficiency analysis and evaluation of energy-saving pressure-compensated circuit for hybrid hydraulic excavator. *Automation in Construction*, 47:62–68, November 2014. ISSN 0926-5805. doi: 10.1016/j.autcon.2014.07.012.

[29] Lennart Werner, Fang Nan, Pol Eyschen, Filippo A. Spinelli, Hongyi Yang, and Marco Hutter. Dynamic Throwing with Robotic Material Handling Machines. In *2024 IEEE/RSJ International Conference on Intelligent Robots and Systems (IROS)*, pages 98–104, 2024. doi: 10.1109/IROS58592.2024.10802743.

[30] Lennart Werner, Pol Eyschen, Sean Costello, Pierluigi Micarelli, and Marco Hutter. Calibrated dynamic modeling for force and payload estimation in hydraulic machinery. *Construction Robotics*, 9(2), October 2025. ISSN 2509-8780. doi: 10.1007/s41693-025-00169-7.

[31] Jiaqi Xu, Bradley Thompson, and Hwan-Sik Yoon. Automated Grading Operation for Hydraulic Excavators. In *SAE Technical Paper 2014-01-2405*, 2014. doi: 10.4271/2014-01-2405.

[32] Teng Yang, Bin Zhang, Haocen Hong, Yuanlong Chen, Huayong Yang, Tongman Wang, and Donghui Cao. Motion control for earth excavation robot based on force pre-load and cross-coupling compensation. *Automation in Construction*, 141:104402, 2022. ISSN 09265805. doi: 10.1016/j.autcon.2022.104402.

[33] Liangjun Zhang, Jinxin Zhao, Pinxin Long, Liyang Wang, Lingfeng Qian, Feixiang Lu, Xibin Song, and Dinesh Manocha. An autonomous excavator system for material loading tasks. *Science Robotics*, 6(55): eabc3164, 2021. doi: 10.1126/scirobotics.abc3164.

[34] John G Ziegler and Nathaniel B Nichols. Optimum settings for automatic controllers. *Transactions of the American society of mechanical engineers*, 64(8):759–765, 1942.